Colloidal Amphiphile Self-Assembly Particles Composed of Gadolinium Oleate and Myverol: Evaluation as Contrast Agents for Magnetic Resonance Imaging

ARTICLE *in* LANGMUIR · OCTOBER 2009

Impact Factor: 4.46 · DOI: 10.1021/la902845j · Source: PubMed

Langmuir Article

pubs.acs.org/Langmuir

Published 2009 by the American Chemical Society

Colloidal Amphiphile Self-Assembly Particles Composed of Gadolinium Oleate and Myverol: Evaluation as Contrast Agents for Magnetic Resonance Imaging

Guozhen Liu,[†] Charlotte E. Conn,[†] Lynne J. Waddington,[‡] Stephen T. Mudie,[§] and Calum J. Drummond*,[†,§]

[†]*CSIRO Molecular and Health Technologies (CMHT), Private Bag 10, Clayton South MDC, VIC 3169, Australia,* [‡]*CSIRO Molecular and Health Technologies (CMHT), 343 Royal Parade, Parkville, VIC 3052, Australia, and* [§]*CSIRO Materials Science and Engineering (CMSE), Private Bag 33, Clayton South MDC, VIC 3169, Australia*

Received August 2, 2009. Revised Manuscript Received October 8, 2009

Gadolinium oleate has been added at various concentrations to a Myverol inverse bicontinuous cubic phase forming system, and the potential of these systems as magnetic resonance imaging (MRI) contrast agents has been investigated. Differential scanning calorimetry (DSC), small-angle X-ray scattering (SAXS), and cryo-transmission electron microscopy (cryo-TEM) measurements on the Gd oleate/Myverol systems indicate that Gd oleate is at least partially incorporated within the cubic phase of Myverol. However, at Gd oleate concentrations greater than 1 wt %, partial phase separation of the system may occur with the formation of a Gd-oleate-rich lamellar phase as well as the cubic phase. Bulk Gd oleate/Myverol mixtures can be dispersed into stable colloidal dispersions. SAXS and cryo-TEM measurements on these dispersions indicate that the presence of Gd oleate in the Myverol system prevents the formation of cubosomes from the bulk cubic phase. Instead, the dispersion consists of putative Gd-oleate-rich nonswelling lamellar nanoparticles as well as colloidal particles lacking ordered internal structure. In vitro studies on these dispersions demonstrated that the relaxivity of select Gd oleate/Myverol systems is much higher than that of pure Gd oleate, exemplifying the promise of this system type for magnetic resonance imaging. The highest water proton relaxivities (r_1 = 34.2 mM^{-1} s^{-1} and r_2 = 27.3 mM^{-1} s^{-1} at 20 MHz and room temperature) were obtained at a Gd oleate loading concentration of 1 wt %, with a subsequent decrease in relaxivity with increasing Gd oleate concentration. These maximum relaxivities compare favorably with the relaxivities for the commercial contrast agent, Magnevist (r_1 = 4.91 mM^{-1} s^{-1} and r_2 = 6.26 mM^{-1} s^{-1} at 20 MHz and room temperature).

1. Introduction

Magnetic resonance imaging (MRI) is recognized as one of the most important and prominent techniques in diagnostic clinical medicine and biomedical research, offering a powerful and nondestructive way to map structure and function in soft tissues by sampling the amount, flow, and environment of water protons in vivo.[1,2] It is noninvasive and offers excellent spatial resolution; however, the relatively low sensitivity associated with the technique has prompted the development of a new class of pharmacological products, called contrast agents, now used in over 35% of MRI diagnoses.[3] Contrast agents enhance signal intensities and improve specificity by altering the relaxation times of water protons in tissues where they are distributed. They can be divided into two groups depending on whether they effect a change in T_1 (the longitudinal relaxation time) or T_2 (the transverse relaxation time) and are known as positive and negative contrast agents, respectively. Positive contrast agents are mainly paramagnetic materials, such as the Gd(III) ion which has seven unpaired electrons, while negative contrast agents consist mainly of superparamagnetic materials such as Fe_3O_4 (magnetite) nanoparticles. The ability of a specific contrast agent to enhance proton relaxation rates is due to both short-range interactions (inner-sphere relaxation from water molecules directly coordinated to the metal ions) and long-range interactions (outer-sphere relaxation from nearby H-bonded water) which are summarized in the standard Solomon−Bloembergen−Morgan equations.[6] Outer-sphere relaxation interactions remain poorly understood but are considered to be small, and it is generally accepted that the relaxivity is primarily affected by the hydration of the metal ion.[7] The longitudinal and transverse relaxivities, r_1 and r_2, respectively, are usually evaluated "in vitro" by calculating the increase in $1/T_1$ and $1/T_2$ effected per millimole of agent and are typically expressed as a rate (mM^{-1} s^{-1}).[7]

The lanthanide ion Gd^{3+} is by far the most frequently chosen MRI contrast agent because it couples a large magnetic moment with a long electron spin relaxation time.[8] However, the free Gd^{3+} ion has been shown to be toxic in both in vitro and in vivo studies,[9−13] as its radial size is approximately equal to that of the

*Corresponding author. E-mail: calum.drummond@csiro.au.

(1) *The Chemistry of Contrast Agents in Medical Magnetic Resonance Imaging*; John Wiley and Sons: New York, 2001.
(2) Raymond, K. N.; Pierre, V. C. *Bioconjugate Chem.* **2005**, *16*, 3.
(3) Aime, S.; Cabella, C.; Colombatto, S.; Crich, S. G.; Gianolio, E.; Maggioni, F. *Magn. Reson. Imaging* **2002**, *16*, 394.
(4) Aime, S.; Dastru, W.; Crich, S. G.; Gianolio, E.; Mainero, V. *Biopolymers* **2002**, *66*, 419.
(5) Bottrill, M.; Nicholas, L. K.; Long, N. J. *Chem. Soc. Rev.* **2006**, *35*, 557.
(6) Lowe, M. P. *Aust. J. Chem.* **2002**, *55*, 551.
(7) Caravan, P.; Ellison, J. J.; McMurry, T. J.; Lauffer, R. B. *Chem. Rev.* **1999**, *99*, 2293.
(8) Meade, T. J.; Taylor, A. K.; Bull, S. R. *Curr. Opin. Neurobiol.* **2003**, *13*, 597.
(9) Biagi, B. A.; Enyeart, J. J. *Am. J. Physiol.* **1990**, *259*, C515.
(10) Ergun, I.; Keven, K.; Uruc, I.; Ekmekci, Y.; Canbakan, B.; Erden, I.; Karatan, O. *Nephrol., Dial., Transplant.* **2006**, *21*, 697.
(11) Molgo, J.; del Pozo, E.; Banos, J. E.; Angaut-Petit, D. *Br. J. Pharmacol.* **1991**, *104*, 133.
(12) Morcos, S. K. *Catheterization Cardiovasc. Interventions* **2006**, *68*, 812.
(13) Rocklage, S. M.; Worah, D.; Kim, S. H. *Magn. Reson. Med.* **1991**, *22*, 216.

Ca^{2+} ion allowing it to disrupt Ca-mediated signaling. Therefore, it must be sequestered by chelation[7] or encapsulation[14−16] for in vivo use. This reduces the number of water molecules coordinated with Gd^{3+} ions, resulting in a compromised efficacy of the system. Commercial contrast agents are dominated by highly stable gadolinium complexes based on the polyaminocarboxylate ligand.[17] These include the anionic complexes of $Gd(DTPA)^{2-}$ (Magnevist) and $Gd(DOTA)^{-}$ (Dotarem) as well as GD(DTPA-BMA) (Omniscan) and Gd(HP-DO3A) (Prohance) which are neutral compounds based on the structures of the anionic complexes. All four have similar pharmokinetic properties as they distribute nonspecifically throughout the extracellular fluid and are rapidly excreted via the kidneys. As well as the lack of specificity of these clinical contrast agents, they suffer from the shortcomings of limited resolution and relatively low inherent sensitivity.[3] This means they can only be used effectively for applications in areas where they are expected to accumulate in high concentration, and this seriously limits their potential for medical diagnoses. The next generation of contrast agents is therefore being designed to incorporate site-specificity, increased efficacy, higher sensitivity, and a more favorable rate of excretion. Some recent approaches have combined the capability of the contrast agent with nanoparticulate platforms such as silica, quantum dots, liposomes, perfluorocarbon (PFC) emulsions, dendrimers, solid lipids, and Gd_2O_3.[18]

Here, we consider the use of self-assembled amphiphile systems as carriers for the paramagnetic metal. When mixed with water, amphiphiles may self-assemble to form a wide variety of liquid crystalline structures displaying differing degrees of dimensionality. These include lamellar phases (1-D), hexagonal phases (2-D), and bicontinuous cubic phases (3-D).[19] The physicochemical properties of some of these systems, described below, suggest that they may be ideal for select biomedical applications. For example, colloidal amphiphile self-assembly systems based on triglycerides and/or their hydrolysis products can be biocompatible and have been studied extensively during the last two decades as vehicles for drug delivery.[20] In addition, they can form high surface area colloidal particles which can accommodate large amounts of active paramagnetic ions, and their aqueous interior allows for the movement of water into and out of the frame. Additionally, it is possible to modify such particles with targeting molecules in order to increase specificity. Recently, there has been increasing interest in the development of new MRI contrast agents based on liposomes,[21−23] and self-assembly amphiphiles.[24,25] In recent work published by us, we have synthesized a series of lanthanide oleates and assessed their properties as MRI contrast agents.[26] We have shown that Gd oleate can be dispersed in water to form lamellar liquid crystalline sub-micrometer particles. However, the relaxivity of Gd oleate dispersions was shown to be slightly compromised relative to that of the commercially available MRI contrast agent, Magnevist.

We have therefore begun to investigate the inverse bicontinuous cubic phases as potential carriers for MRI contrast agents. The inverse bicontinuous cubic phases consist of a single, continuous bilayer subdividing space into two interpenetrating, but unconnected, water networks. The bilayer midplane may be closely described as a surface of zero mean curvature known as a triply periodic mean surface (TPMS). Cubic lipid phases of unsaturated monoglycerides are characterized by high biocompatibility, bioadhesivity, and easy production protocol.[27] Because of the biological relevance of the cubic phases, their high interfacial area, their stability in contact with excess water, and their capability to solubilize both hydrophilic and hydrophobic active molecules, there is great interest both in their complex phase behavior and in the utilization of these colloidal dispersions for formulating particulate drug delivery systems in pharmacological applications.[28,29] Previous research has shown that these versatile delivery systems can be administered orally, parenterally, or percutaneously.[30−32]

Here, we concentrate on the well-characterized lipid system Myverol.[33] This contains 82% monoacylglycerols (86.6% monoolein, 7.0% monostearin, 3.5% monopalmitin, 0.9% monoarachidin, and 2.0% unidentified) and displays a rich phase diagram which includes not only an inverse bicontinuous Q_{II}^{D} cubic phase but also a fluid lamellar phase (L_α), an inverse hexagonal phase (H_{II}), and a fluid isotropic phase (L_2).[33] The phase behavior of Myverol in the presence of a wide range of different hydrophilic and hydrophobic guest molecules has been widely studied along with the biological and pharmaceutical relevance of these systems.[34−36] In this study, we aim to investigate potential MRI contrast agents by incorporating Gd oleate within Myverol, forming a binary system. The phase behavior of the Gd oelate/Myverol system was investigated. Dispersions of Gd oleate/Myverol in water were found to form structure-containing, nanosized particles ranging from 200 to 400 nm. Small angle X-ray diffraction and cryo-transmission electron microscopy were used to characterize the internal structure of these dispersed particles. We observe that select dispersions have substantially improved relaxivities compared with the aqueous dispersions of pure Gd oleate investigated in our previous paper.[26]

2. Experimental Section

Materials and Chemicals. All chemicals were used as received, without further purification. Pluronic F127 ($PEO_{99}-PPO_{67}-PEO_{99}$) was obtained from BASF Corporation (Sigma).

(14) Kato, H.; Kanazawa, Y.; Okumura, M.; Taninaka, A.; Yokawa, T.; Shinohara, H. *J. Am. Chem. Soc.* **2003**, *125*, 4391.
(15) Bolskar, R. D.; Benedetto, A. F.; Husebo, L. O.; Price, R. E.; Jackson, E. F.; Wallace, S.; Wilson, L. J.; Alford, J. M. *J. Am. Chem. Soc.* **2003**, *125*, 5471.
(16) Sitharaman, B.; Kissell, K. R.; Hartman, K. B.; Tran, L. A.; Baikalov, A.; Rusakova, I.; Sun, Y.; Khant, H. A.; Ludtke, S. J.; Chiu, W.; Laus, S.; Toth, E.; Helm, L.; Merbach, A. E.; Wilson, L. J. *Chem. Commun.* **2005**, 3915.
(17) Weimann, H.-J.; Ebert, W.; Misselwitz, S.; Schmitt-Willich, H. *Eur. J. Radiol.* **2003**, *46*, 33.
(18) Sharma, P.; Brown, S. C.; Walter, G.; Santra, S.; Scott, E.; Ichikawa, H.; Fukumori, Y.; Moudgil, B. M. *Adv. Powder Technol.* **2007**, *18*, 663.
(19) Kaasgaard, T.; Drummond, C. J. *Phys. Chem. Chem. Phys.* **2006**, *8*, 4957.
(20) Drummond, C. J.; Fong, C. *Curr. Opin. Colloid Interface Sci.* **1999**, *4*, 449.
(21) Mulder, W. J. M.; Strijkers, G. J.; Griffioen, A. W.; Bloois, L.; Molema, G.; Storm, G.; Koning, G.; Nicolay, K. *Bioconjugate Chem.* **2004**, *15*, 799.
(22) Leclercq, F.; Cohen-Ohana, M.; Mignet, N.; Sbarbati, A.; Herscovici, J.; Scherman, D.; Byk, G. *Bioconjugate Chem.* **2003**, *14*, 112.
(23) Ayyagari, A. L.; Zhang, X.; Ghaghada, K. B.; Annapragada, A.; Hu, X.; Bellamkonda, R. V. *Magn. Reson. Med.* **2006**, *55*, 1023.
(24) Bull, S. R.; Guler, M. O.; Bras, R. E.; Meade, T. J.; Stupp, S. I. *Nano Lett.* **2005**, *5*, 1.
(25) Bull, S. R.; Guler, M. O.; Bras, R. E.; Venkatasubramanian, P. N.; Stupp, S. I.; Meade, T. J. *Bioconjugate Chem.* **2005**, *16*, 1343.
(26) Liu, G.; Conn, C. E.; Drummond, C. J. *J. Phys. Chem. B* **2009**; DOI: 10.1021/jp906344u.
(27) Larsson, K. *Curr. Opin. Colloid Interface Sci.* **2000**, *5*, 64.
(28) Shah, J. C.; Sadhale, Y.; Chilukuri, D. M. *Adv. Drug Delivery Rev.* **2001**, *47*, 229.
(29) Siekmann, B.; Bunjes, H.; Koch, M. H.; Westesen, K. *Int. J. Pharm.* **2002**, *244*, 33.
(30) Chung, H.; Kim, J.; Um, J. Y.; Kwon, I. C.; Jeong, S. Y. *Diabetologica* **2002**, *45*, 448.
(31) Engstrom, S.; Ericsson, B.; Landh, T. *Proc. Int. Symp. Controlled Release Bioact. Mater.* **1996**, *23*, 382.
(32) Kim, J. S.; Kim, H. K.; Chung, H.; Sohn, Y. T.; Kwon, I. C.; Jeong, S. Y. *Proc. Int. Symp. Controlled Release Bioact. Mater.* **2000**, *27*, 1118.
(33) Clogston, J.; Rathman, J.; Tomasko, D.; Walker, H.; Caffrey, M. *Chem. Phys. Lipids* **2000**, *107*, 191.
(34) Caboi, F.; Amico, G. S.; Pitzalis, P.; Monduzzi, M.; Nylander, T.; Larsson, K. *Chem. Phys. Lipids* **2001**, *109*, 47.
(35) Caboi, F.; Murgia, S.; Monduzzi, M.; Lazzari, P. *Langmuir* **2002**, *18*, 7916.
(36) Caboi, F.; Nylander, T.; Razumas, V.; Talaikyte, Z.; Monduzzi, M.; Larsson, K. *Langmuir* **1997**, *13*, 5476.

Myverol 18−99 K was purchased from Quest International (Bronson & Jacobs, Australia). Gd oleate was synthesized according to the literature.[26]

Sample Preparation. Myverol and Gd oleate were weighed and dissolved in hot chloroform. The solvent was evaporated by freeze-drying overnight to form the final binary Myverol/Gd oleate mixture.

Differential Scanning Calorimetry. Differential scanning calorimetry (DSC) measurements were performed on a Mettler 3000 system. Solid samples weighing 5−10 mg were sealed in aluminum pans (25 μL) with pierced lids and heated or cooled at a scan rate of 2.5−10 °C min^{-1}. Thermograms were recorded under a nitrogen atmosphere, using empty aluminum pans as the reference. An indium standard was used to calibrate the DSC temperature (±0.3 °C) and enthalpy scale. The energies and peak temperatures of the transitions were determined using the Mettler 3000 software package. The glass transition, T_g, was determined at the point where the extrapolated lines from the baseline and the glass transition "cliff" intersected.

Water Penetration Scans. Mixtures of Myverol and Gd oleate were melted between a microscope slide and coverslip and then cooled to room temperature. Water added at the edge of the coverslip is drawn between the two glass surfaces and surrounds the solidified material by capillary action. The sample was heated in increments of 5 °C with equilibration times of 30 min in a Mettler FP82HT hot stage controlled by a FP90 programmable processor. Optical textures were observed with an Olympus IMT-2 cross-polarized optical microscope.

Formulation of Myverol/Gd Oleate Aqueous Dispersions. Mixtures of Myverol and Gd oleate were dispersed in excess Milli-Q water to form particles. A total of 0.05 g (10 w/w%) of stabilizer Pluronic F127 was added to 0.5 g of the molten Myverol/Gd oleate binary mixture. This was added slowly to 50 mL of Milli-Q water with mixing under ultratarrax (Polytron PT 10-35 GT, KINEMATICA, Switzerland) for 5 min at a speed of 15 000 rpm at 80 °C. The dispersion was immediately passed through a high pressure homogenizer (Avestin, Germany) using pressures of 10 000 psi for six passes at 60 °C. The solution appeared milky, indicating the formation of colloidal particles. The obtained particles were sized by dynamic light scattering measurements (COULTER LS230 particle size analyzer).

Small-Angle X-ray Scattering (SAXS) Measurements. The structures of the bulk phases in excess water were determined using small-angle X-ray scattering. Samples were loaded into a small sample cell consisting of two very thin mica windows separated by a 1 mm stainless steel spacer ring and loaded into a custom built sample holder within the SAXS instrument chamber. The SAXS system employed was developed by Osmic Inc. (Rigaku Group). This camera uses a Cu Kα (λ = 1.5408 Å) microfocus source, with a graded multilayer optic to increase flux and monochromate the X-ray beam. For these experiments, the camera was configured with a three pinhole geometry for beam collimation, giving a spot size of 0.26 mm fwhm at the sample position. Throughout the experiments, the sample chamber was at atmospheric pressure; however, in order to minimize air scatter, a cone shaped attachment extended the post-sample flight tube into the sample chamber, thus reducing the air path length to approximately 3 cm. Beryllium windows separated the evacuated collimation and post-sample flight tubes from the sample environment. A computer controlled $x-y$ translation stage, mounted inside the sample chamber, was used for sample alignment, with a small photonic science CCD acting as a beam monitor. Fujifilm imaging plates (BAS-MS) and scanner (BAS 5000) were used to collect and read out the SAXS patterns. The imaging plates were mounted in vacuum during exposure, with a sample to imaging plate distance of approximately 1.6 m. The effective q-range of this system is 0.007−0.27 Å^{-1}. A silver behenate standard was used to calibrate the reciprocal space vector. Data reduction (calibration and integration) was achieved using the SAXS15ID software package.[37]

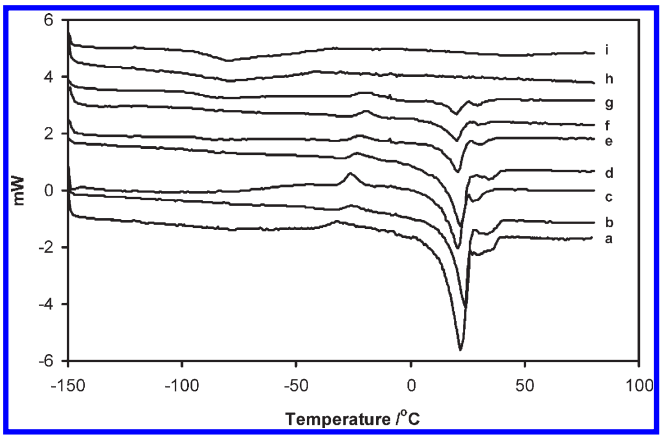

Figure 1. Differential scanning calorimetry curves for Myverol/Gd oleate mixtures with (a) 0%, (b) 10%, (c) 20%, (d) 30%, (e) 40%, (f) 50%, (g) 60%, (h) 80%, and (i) 100% wt % Gd oleate at a scan rate of 2.5 °C min^{-1}.

SAXS experiments were also performed on dispersed samples. As diffraction from such samples tends to be weak, data were collected at the 15-ID-D (ChemMatCARS) beamline of the Advanced Photon Source, Argonne, IL.[37] The experiments used a beam of wavelength λ = 1.50 Å (8.27 keV) with dimensions 200 μm × 100 μm and a typical flux of 1 × 10^{12} photons s^{-1}. Two-dimensional diffraction images were recorded on a Bruker 6000 CCD detector with an active area of 94 × 94 mm^2 and a pixel size of 92 μm. The CCD detector was offset from the main beam allowing analysis in the q-range 0.0187−0.807 Å^{-1} at a sample to detector distance of 0.6 m. Temperature control was in the range 7−90 °C. Image analysis was carried out using AXcess, an IDL-based software package developed by Dr. Andrew Heron at Imperial College London.[38]

Cryo-Transmission Electron Microscopy (Cryo-TEM) Studies. The samples were prepared for cryo-TEM as follows: 4 μL of sample was applied to a 300-mesh copper grid coated with lacey Formvar-carbon film (ProSciTech) or C-Flat perforated carbon film (Protochips Inc.) and allowed to settle for 30 s. The grid was then blotted for 2−10 s, with blotting time being optimized for each sample, and immediately plunged into liquid ethane. The humidity and temperature in the plunging device (a home-built device) were 65% and 22 °C, respectively. The frozen and vitrified grids were stored in liquid nitrogen before being transferred into a Gatan 626 DH cryo holder and then imaged in a FEI Tecnai 12 transmission electron microscope operating at 120 KV. Images were obtained using an Olympus MegaView III CCD camera and AnalySis camera control software, employing low-dose procedures at all times. The samples was imaged at −182 °C, at a defocus level of approximately 2 μm for all samples. The electron dose was kept to under 1000 electrons nm^{-2} (10 electrons Å^{-2}), and the magnification used varied from ×40k to ×97k.

Relaxation Time Measurement. Stock solutions of Myverol/Gd oleate aqueous dispersions were diluted in Milli-Q water to form a series of solutions with variable Gd oleate concentration. Relaxivities were calculated from a graph of the inverse of the relaxation time versus the concentration of Gd oleate in Myverol.

The longitudinal and transverse relaxation time, T_1 and T_2, of the dispersed samples were measured at room temperature using a 20 MHz MINISPEC. Dispersions were made using the method

(37) Cookson, D.; Kirby, N.; Knott, R.; Lee, M.; Schultz, D. *J. Synchrotron Radiat.* **2006**, *13*, 440.
(38) Seddon, J. M.; Squires, A. M.; Conn, C. E.; Ces, O.; Heron, A. J.; Mulet, X.; Shearman, G. C.; Templer, R. H. *Philos. Trans. R. Soc., A* **2006**, *364*, 2635.

Table 1. Glass Transition Temperature (T_g), Melting Temperature (T_m), and Solid−Solid Transition Temperature (T_p) for Various Myverol/Gd Oleate Mixtures[a]

% of Gd oleate in Myverol	T_g (°C)	T_p (°C) [ΔH (J g^{-1})]	$T_m(1)$ (°C) [ΔH (J g^{-1})]	$T_m(2)$ (°C) [ΔH (J g^{-1}]
0	NO	−32.4 [2.1]	20.6 [−51.7]	35.8 [−5.57]
10	NO	−28.6 [4.4]	20.2 [−45.6]	34.0 [−4.8]
20	NO	−25.8 [7.6]	19.6 [−41.8]	30.8 [−3.1]
30	NO	−22.3 [5.2]	19.0 [−36.6]	30.4 [−2.9]
40	NO	−21.9 [4.6]	18.8 [−23.1]	30.2 [−2.7]
50	NO	−20.0 [3.6]	18.6 [−15.18]	29.6 [−2.2]
60	−93.2 (−88.1)	−19.7 [3.1]	18.3 [−7.3]	29.1 [−1.7]
80	−92.1 (−84.8)	NO	NO	NO
100	−91.8 (−83.0)	NO	NO	NO

[a] The transition enthalpies are given in square brackets. Note that for T_g the onset temperature is given with the midpoint given in brackets. NO indicates that a particular transition was not observed.

described above. For T_1 measurements, the standard inversion−recovery (IR) method was used as the pulse sequence.[39] The recycle delay time was set to five times the T_1 value. Typically, 20 points were taken for each T_1 measurement. For T_2 measurements, the Carr−Pucell−Meiboom−Gill (CPMG) method was used.[39]

3. Results and Discussion

3.1. Structure of the Bulk Samples. *Differential Scanning Calorimetry*. DSC scans at a heating rate of 2.5 °C min^{-1} over the range of −150 to +80 °C are presented in Figure 1 for dry mixtures of Myverol and Gd oleate. The transition temperatures and enthalpies for the transitions are listed in Table 1. Previous XRD data on pure Myverol, which consists of a mixture of lipids, indicated that the system continuously melts over a range of temperatures between 0 and 35 °C.[33] Here, we find that the pure Myverol system displays a large endothermic peak at 20.6 °C along with a broad undefined peak centered at approximately 35.8 °C. We denote these $T_m(1)$ and $T_m(2)$ and attribute them to a broad melting of the system over a range of temperatures. Upon addition of up to 60 wt % Gd oleate to the system, we note that the DSC curve maintains approximately the same shape but that the temperatures at which $T_m(1)$ and $T_m(2)$ occur decrease. The enthalpy of both peaks is also observed to decrease with increasing concentration of Gd oleate, and by 80 wt % Gd oleate the enthalpy of melting is so low that a melting point is not detected on the DSC trace. However, previous research by us has shown that pure Gd oleate melts at approximately 37 °C.[26] For samples up to 60 wt % Gd oleate, an additional exothermic transition (denoted T_p) is observed at temperatures between approximately −30 °C and −20 °C and attributed to a solid−solid transition within the sample. This is consistent with previous X-ray data on the pure Myverol system which indicated that it forms at least two crystalline lamellar polymorphs.[33] The temperature of this transition increases with increasing weight ratio of Gd oleate (Table 1). For those mixtures which were high in Gd oleate, an additional glass transition (T_g) is observed at approximately −90 °C.

We note that the enthalpy change associated with the $T_m(1)$ transition displays an approximately linear relationship with weight percent Gd oleate (Figure 2) (we were unable to comment similarly on the $T_m(2)$ transition due to the extremely broad nature of the peak). This could be an indication either that the Gd oleate is mixing ideally with the Myverol system or, conversely, that it is not mixing at all.

Lyotropic Phase Behavior Using Polarizing Microscopy. Water penetration scans involving the direct observation of the birefringence of lyotropic phases via cross-polarized microscopy

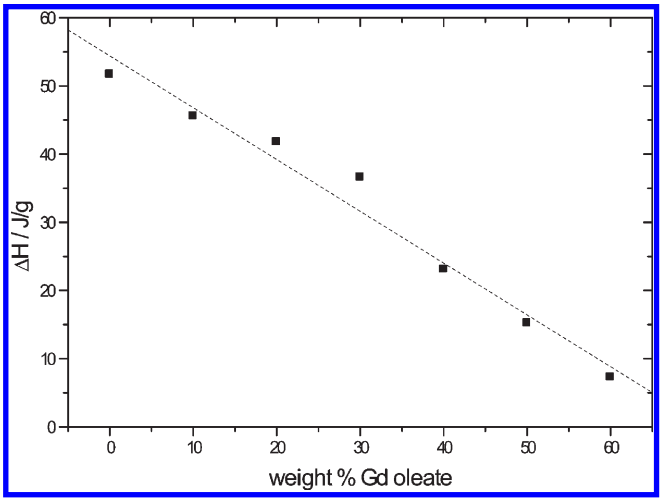

Figure 2. Enthalpy change associated with the $T_m(1)$ melting peak as a function of weight percent Gd oleate.

were initially used to determine the number of mesophases formed at specific temperatures along with their lyotropic phase behavior. Under crossed polarizers, anisotropic phases such as the lamellar and hexagonal phases are birefringent and display well-characterized textures while cubic and micellar phases appear as dark bands. Representative water penetration scans of various Myverol/Gd oleate mixtures at 25 °C are shown in Figure 3. The particular mesophases observed with increasing water content and the temperature window over which each is seen are listed in Table 2.

The phase sequence displayed by the Myverol/water system is shown in Figure 3a. At room temperature, a viscous isotropic Q_{II} phase, attributed to an inverse bicontinuous cubic structure, quickly developed in contact with water, with a second anisotropic phase observed between this phase and the surfactant crystals. The anisotropic phase was assigned as a fluid lamellar (L_α) phase based on its optical texture. A poorly defined narrow isotropic band observed between the L_α phase and solid crystal sample is attributed to a low water content fluid micellar phase (L_2). The phase sequence on increasing water content at room temperature is generally consistent with the published literature on Myverol.[33] The absence of a second cubic phase at lower water contents predicted by the phase diagram reflects difficulties in distinguishing refractive index differences between the two cubic phases, and we note that both cubic phases are clearly differentiated in the absence of crossed polarizers (unpublished data).

We observe that Gd oleate can be incorporated into this system up to a concentration level of 50 wt % while retaining the same phase sequence on increasing water. However, with increasing Gd oleate concentration, the L_α and Q_{II} bands become progressively

(39) *Modern NMR Techniques for Chemistry Research*; Derome, A. E., Ed.; Pergamon Press: Oxford, 1987; Vol. 6, p 86.

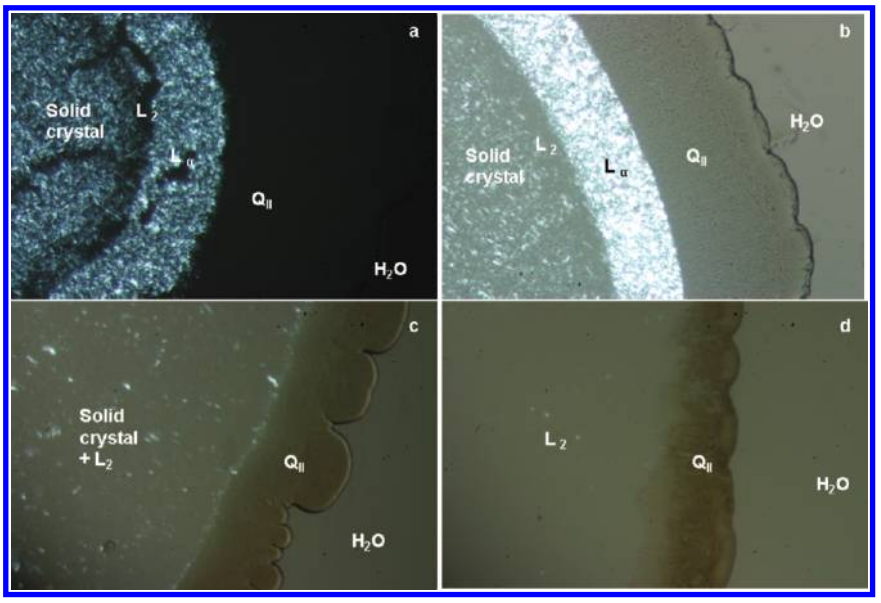

Figure 3. Optical microscope images of water penetration into (a) pure Myverol and (b) 10%, (c) 40%, and (d) 60% Gd oleate in Myverol at 25 °C.

narrower, indicating that these mesophases are observed over a smaller concentration range. The effect seems to be more pronounced for the L_α phase, which exists over a very narrow concentration range by 40 wt % Gd oleate. The cubic phase was not observed above a Gd oleate weight ratio of 60%. We also observe that at higher Gd oleate contents the pure crystal phase more easily transforms to a fluid micellar phase, L_2. At 40% Gd oleate, the system has partially formed the fluid micellar phase with patches of crystal observed. By 60% Gd oleate, no solid crystal phase is observed. We note that these last two observations may reflect supercooling of the system.

The thermal behavior of these systems was investigated at various Gd oleate concentrations. We describe the system at 10 wt % Gd oleate as an example. As described above, at room temperature, the system displays the phase sequence $L_c-L_2-L_\alpha-Q_{II}$ with increasing water content. Upon increasing the temperature, no change in phase sequence was observed until 40 °C. On standing at this temperature, the initial lamellar phase was replaced by a fanlike texture phase, which is characteristic of the inverse hexagonal phase (H_{II}) as described by Laughlin.[40] The cubic phase disappeared completely around 55 °C. With further heating, fingers of water invaded the central area and converted the entire sample to an inverse hexagonal phase which melted around 80 °C. The change in phase sequence with temperature is listed in Table 2 for all concentrations studied. In general, the cubic and lamellar phases disappear earlier as the Gd oleate concentration is increased, again indicating that these phases are destabilized in the presence of Gd oleate. The temperature at which the H_{II} phase is first observed also increases with increasing Gd oleate concentration.

Lyotropic Phase Behavior Using SAXS. SAXS experiments were carried out to provide a definitive phase assignment for each of the phases observed with cross-polarized microscopy as well as a lattice parameter for each phase. Data were collected for a range of compositions of the Myverol/Gd oleate surfactant system in excess water at room temperature. Some representative raw 2-D images are shown in Figure 4. These images were azimuthally integrated to produce 1-D plots of intensity versus scattering vector q. These 1-D plots can be stacked, allowing changes in relative peak intensities and positions to be more easily visualized, and are shown in Figure 5 for all concentrations studied.

Table 2. Lyotropic Phase Behavior of Myverol/Gd Oleate Mixtures as a Function of Temperature[a]

% of Gd oleate in Myverol	temperature range of L_c phase (°C)	temperature range of L_α phase (°C)	temperature range of Q_{II} phase (°C)	temperature range of H_{II} phase (°C)
0	<24−35	<24−40	<24−55	<40−85
1	<24−35	<24−40	<24−55	<45−80
5	<24−35	<24−40	<24−55	<45−80
10	<24−35	<24−35	<24−55	<45−80
20	<24−30	<24−35	<24−50	<45−80
30	<24−30	<24−35	<24−50	<45−80
40	<24−30	<24−35	<24−45	<50−75
50	<24−30	<24−35	<24−45	<50−75
60	<24−35	NO	NO	NO
80	<24−35	NO	NO	NO
100	<24−35	NO	NO	NO

[a] NO indicates that a particular phase was not observed over the temperature range studied.

Pure Myverol forms a Q_{II}^D cubic phase (crystallographic space group *Pn3m*) at room temperature, and characteristic peaks in the ratio $\sqrt{2}$, $\sqrt{3}$, $\sqrt{4}$, $\sqrt{6}$, $\sqrt{8}$, and $\sqrt{9}$ are seen in the 2-D diffraction pattern (Figure 4a). At 1% Gd oleate, a single Q_{II}^D phase structure is retained (Figure 4b). At concentrations of Gd oleate > 1%, a second phase is seen in the diffraction pattern (Figure 4c). Peaks corresponding to the Q_{II}^D cubic phase are retained, but two extra peaks are observed at approximately q = 0.133 and 0.266 Å^{-1}, characteristic of a lamellar phase of approximate lattice parameter 47 Å. The intensities of the lamellar peaks increase relative to those of the Q_{II}^D peaks as the Gd oleate concentration is increased (Figure 5), indicating that the lamellar phase grows at the expense of the cubic phase with increasing Gd oleate concentration. By 80% Gd oleate, peaks corresponding to the Q_{II}^D phase have disappeared completely. Lattice parameters for both the cubic and lamellar phases were calculated using regression analysis, and they are listed in Table 3. The lattice parameter of the lamellar phase (46.6−47.3 Å) is similar to that displayed by pure Gd oleate (46.4 Å) which forms a gel lamellar (L_β) phase at room temperature.[26] Such behavior

(40) Laughlin, R. E. *The Aqueous Phase Behaviour of Surfactants*; Academic Press: Cambridge, U.K., 1996.

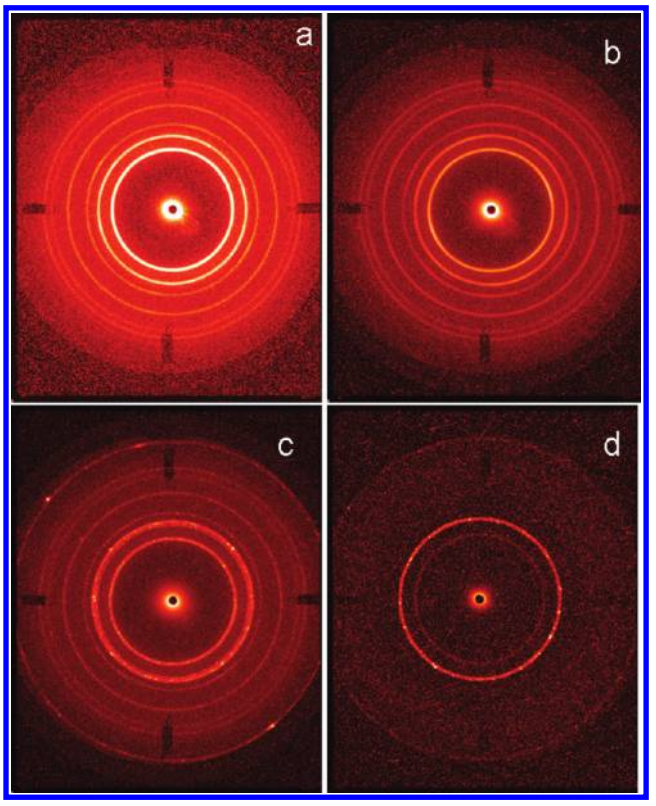

Figure 4. Representative small-angle X-ray diffraction patterns for (a) pure Myverol, (b) 1% Gd oleate in Myverol, (c) 20% Gd oleate in Myverol, and (d) 60% Gd oleate in Myverol. All samples were run under excess water conditions at room temperature.

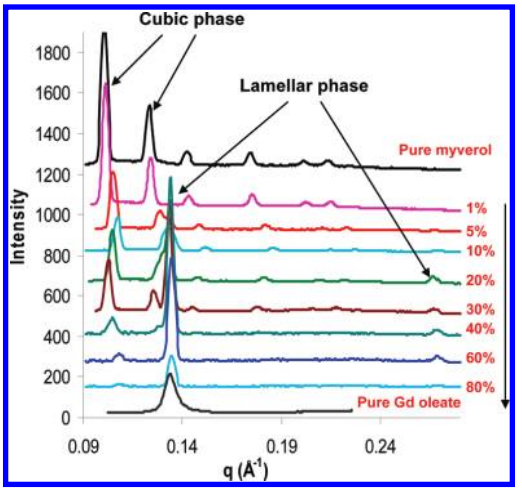

Figure 5. Stacked plot showing 1-D profiles of intensity versus q for bulk mixtures of Myverol and Gd oleate saturated with excess water.

may suggest that while Gd oleate is incorporated within the Myverol cubic phase at lower concentrations, at higher concentrations partial phase separation of the Gd oleate from the Myverol may have occurred with the Gd oleate preferentially forming the lamellar phase rather than penetrating the Myverol cubic phase. We note that such phase separation is not observed visually during optical microscopy experiments on Myverol/Gd oleate mixtures and suggests that pockets of Gd-oleate-rich phase may form on a mesoscale level and remain dispersed throughout the cubic phase. This is discussed further in section 3.3.

Table 3. Lattice Parameters Determined from SAXS Profiles of Gd Oleate/Myverol Mixtures under Excess Water Conditions[a]

% of Gd Oleate in Myverol	Q_{II}^{D} lattice parameter (Å) (bulk phase)	lamellar lattice parameter (Å) (bulk phase)	lamellar lattice parameter (å) (Dispersed phase)
0	88.4		
1	87.8		48.0
5	84.7	47.3	46.7
10	82.7	46.7	47.3
20	84.5	47.1	46.9
30	86.7	47.2	NP
40	84.7	46.8	NP
60	82.5	46.7	NP
80		46.6	NP
100		46.4	46.4[b]

[a] NP indicates that a SAXS measurement was not performed. [b] This value was obtained from ref 23.

The 2-D diffraction images displayed in Figure 4 show marked changes in the "granularity" of diffraction rings with increased weight ratio of Gd oleate. Samples of pure Myverol and Myverol containing 1% Gd oleate display smooth diffraction rings indicating a random powderlike grain orientation within these samples and placing an upper limit on grain size of 1 μm. Above 1% Gd oleate, we note increasing granularity (or spots) within the diffraction rings corresponding to both the cubic and lamellar phases. This indicates either that the average grain size has increased in the presence of Gd oleate or that this has caused some preferential alignment of the grains within the sample.

3.2. Structure of the Dispersed Samples. SAXS results described above for the bulk phase of Myverol/Gd oleate under excess water conditions indicate that, depending on the concentration of Gd oleate, mixtures of Gd oleate and Myverol self-assemble into coexisting nanostructured cubic and lamellar phases. The paramagnetic nature of Gd suggests that such a system might have potential as a contrast agent for magnetic resonance imaging. However, for biomedical applications, such systems must be dispersed into sub-micrometer sized particles for delivery within the body. Hence, we have dispersed these systems as colloidal particles using the methods described in the Experimental Section and show that they form stable colloidal dispersions of self-assembled amphiphiles. The particle size distributions (D_{10}, D_{50}, D_{90}) for these dispersions are provided in Table 4. When the concentration of Gd oleate in Myverol is below 50%, dispersions of mixtures of Gd oleate and Myverol form nanoparticles with a particle size of approximately 300 nm. As the Gd oleate loading increases above this, the average nanoparticle size also increases, with an average particle size of approximately 1 μm for 100% Gd oleate samples. It is known that larger nanoparticle sizes pose special issues when used in vivo. However, as discussed in the following sections, low relaxivity values associated with higher Gd oleate loadings render such dispersions unlikely to be used in vivo. Additionally, nanoparticle sizes may be minimized by dispersion processing method optimization, although this has not been explored in the current study.

SAXS on Dispersed Samples. SAXS experiments were carried out on dispersed samples containing Gd oleate in the weight ratios 1%, 5%, 10%, and 20% to confirm that long-range structural order is present and to obtain accurate d-spacings. Due to the weak scattered intensity typically obtained from dispersions, experiments were carried out at a synchrotron radiation facility as described earlier. Samples were run at 25 °C for comparison with previous SAXS and XRD data on the bulk samples and at 37 °C for physiological relevance.

Table 4. Colloidal Particle Sizes and Relaxivities of Myverol/Gd Oleate Mixtures Dispersed in Water[a]

	particle size (nm)			relaxivity (mM^{-1} s^{-1})	
% of Gd oleate in Myverol	D_{10}	D_{50}	D_{90}	r_1	r_2
0	102	158	235		
0.1	161	291	486	15.62	22.17
0.5	171	302	485	20.29	26.06
1	68	226	410	34.24	27.34
5	82	143	230	19.01	26.11
10	97	236	470	13.60	20.30
20	128	275	488	9.31	13.35
30	173	323	860	4.71	7.64
40	86	204	854	3.59	6.16
50	185	473	1313	2.82	5.39
60	256	599	1473	1.86	4.21
80	393	691	1893	1.72	3.81
100	359	932	1956	2.78	6.06
Magnevist				4.91	6.26

[a] Relaxivities were measured by MINISPEC at 0.5 T (20 MHz) at room temperature.

Diffraction patterns for the above samples at 25 °C are shown in Figure 6. Above 1 wt % Gd oleate, SAXS experiments indicate that the bulk Myverol/Gd oleate mixture forms coexisting lamellar and cubic phases. Here, two distinct peaks corresponding to a dispersed lamellar phase of approximate lattice parameter 47 Å are seen for all samples. The lattice parameters, given in Table 3, are similar to those seen for the bulk samples indicating that the lamellar phase has dispersed well into sub-micrometer particles. However, we do not see peaks corresponding to a dispersed cubic phase. Rather, a band of diffuse scatter, seen at a *d*-spacing of approximately 41 Å and indicating the presence of some disorder within the dispersed sample, suggests that the structure of the cubic phase has been impacted.

SAXS results described here are in agreement with cryo-TEM results on the dispersed samples described in the following section. We note that, although pure Myverol forms cubosomes, addition of even the smallest amount of Gd oleate seems to disrupt cubosome formation.

Cryo-TEM Studies. Cryo-TEM analyses have been conducted on dispersions of Myverol/Gd oleate at 0, 0.1, 1, 5, 10, and 20 wt % Gd oleate. Representative cryo-TEM micrographs for a pure Myverol sample and Myverol samples containing 0.1, 1, and 20 wt % Gd oleate are shown in Figure 7. For the pure Myverol sample (Figure 7a), we observe many well-shaped cubosome particles exhibiting the typical ordered cubic texture along with numerous transparent spherical unilamellar vesicles. The cubosomes are approximately 150−200 nm in diameter and are therefore composed of the order of 20−25 unit cells. Water storage at the edges of the cubosomes can be clearly seen. Upon addition of 0.1% Gd oleate, the cubosome structure is disrupted. We observe (Figure 7b) many residual cubosome-like structures with the loss of internal order. In all cases, the residual cubosome structures appear to be bounded by one or many double walled vesicles. The unilamellar vesicles observed for the pure Myverol dispersion are still visible.

Cryo-TEM images for samples containing 1, 5, 10, and 20 wt % Gd oleate are very similar. Very few residual cubosome-like structures are seen, and these become less numerous as the concentration of Gd oleate is increased. Rather we begin to observe numerous spherical vesicles with a structure consisting of irregular concentric rings like the layers of an onion. These structures, similar to multilamellar vesicles, coexist with the double walled and unilamellar vesicles previously observed (Figure 7c) and are in the size range 50−300 nm. Approximate

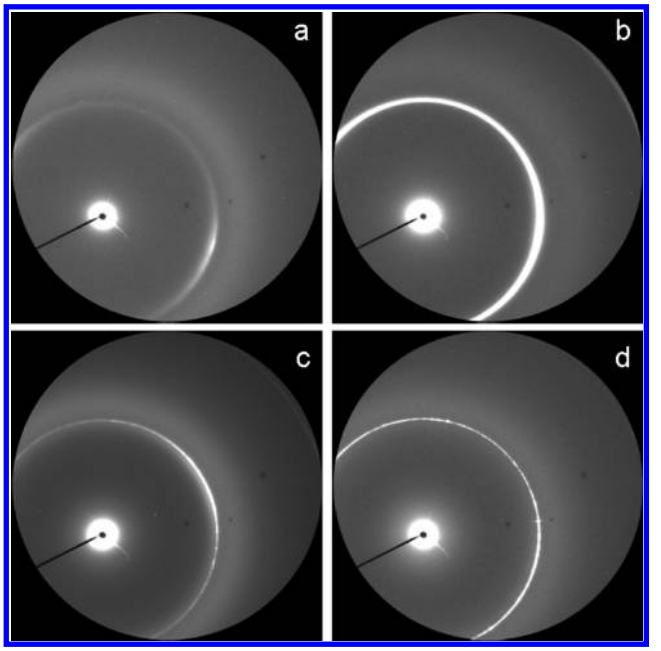

Figure 6. Representative small-angle diffraction patterns from dispersed samples of Myverol containing Gd oleate at (a) 1%, (b) 5%, (c) 10%, and (d) 20%. For all images, the first and second order lamellar reflections are seen as well as a broad ring of diffuse scatter.

layer spacings extracted from the cryo-TEM images are in the range 47−51 Å, which is similar to the *d*-spacing of the lamellar reflections observed in the SAXS patterns of the dispersed samples (46.7−48.0 Å). As the concentration of Gd oleate is increased, and the number of residual cubosomes observed decreases, we observe an increase in the number of multilamellar vesicles. We note also that these multilamellar vesicles are highly similar to those observed in a dispersed sample of pure Myverol which has degraded with age (unpublished data). We therefore suggest that the presence of Gd oleate is disrupting the formation of cubosomes in the Myverol system and promoting instead the formation of these multilamellar vesicles.

For all samples with Gd oleate > 1 wt %, there are widespread sheetlike structures which appear as irregular sheets at first but take on a rhombus-shaped crystalline appearance as the concentration of Gd oleate increases (Figure 7d). Most of the particles are highly opaque or electron-dense, suggesting that they all contain Gd. These particles and sheets are very beam-sensitive, with extensive radiation damage occurring after less than 2 s of beam exposure. We suggest that such structures are nondispersed crystalline Gd oleate confirming that partial phase separation has occurred within the system. We also note that the sheets were not observed by optical microscopy or dynamic light scattering measurements on the colloidal dispersions and therefore may be a cryo-TEM preparation induced crystallization phenomenom.

3.3. Discussion. We have characterized the Myverol/Gd oleate system both in bulk and dispersed form using a combination of DSC, SAXS, cross-polarized microscopy, and cryo-TEM measurements. SAXS measurements on the bulk systems indicate that coexisting lamellar and cubic phases are formed at Gd oleate contents > 1 wt %. The similarity between the lattice parameter formed by the lamellar phase with that formed by pure Gd oleate suggests that the coexisting lamellar phase is highly rich in Gd oleate, indicating that at least partial phase separation has occurred between the Myverol and Gd oleate systems. This is backed up by cryo-TEM measurements on the dispersed samples

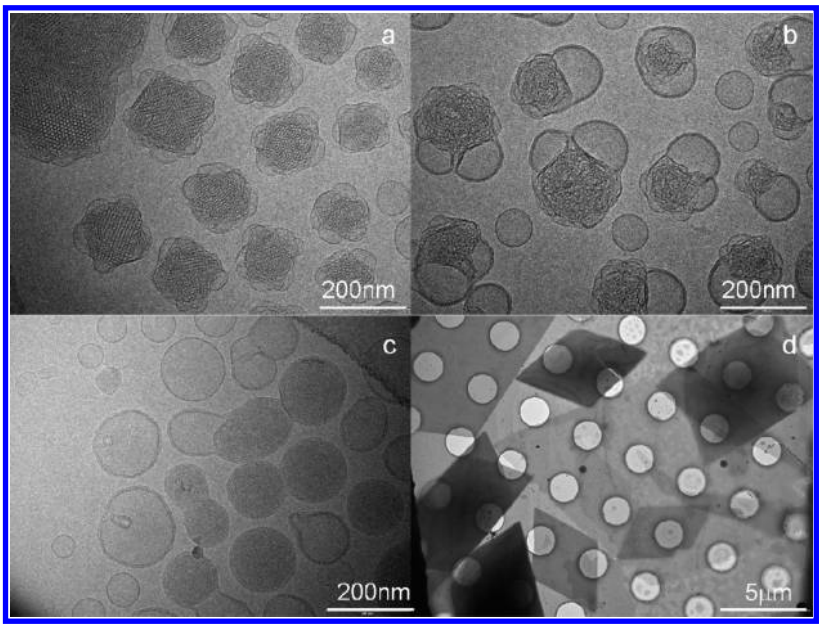

Figure 7. Cryo-transmission electron microscopy images for dispersions of (a) pure Myverol, (b) 0.1% Gd oleate in Myverol, (c) 1% Gd oleate in Myverol, and (d) 20% Gd oleate in Myverol. In (d), crystalline sheets are overlaying holes in the cryo-TEM grid.

where, again for Gd oleate concentrations > 1%, multilamellar particles similar to the nonswelling lamellar nanoparticles seen for pure Gd oleate are noted.[26] However, DSC measurements on the same samples indicated that the temperatures of all observed transitions (including two melting transitions and a crystal−crystal transition) change continuously as the Gd oleate concentration is increased up to a Gd oleate concentration of 60 wt %. In addition, cross-polarized microscopy images show that the phase sequence on increasing water adopted by pure Myverol is retained up to 50 wt % Gd oleate but with a narrowing of the concentration range over which the cubic and lamellar phases are seen. All of the above results suggest that Gd oleate continues to incorporate within the Myverol system to some extent as the concentration is increased above 1%.

We suggest that Gd oleate has been partially incorporated within the Myverol system but are unable to comment definitively as to the level at which this occurs. At low levels, Gd oleate may be incorporated within the Myverol bilayer in molecular form. This will affect the lattice parameter of the system and, at high enough levels, may disrupt the overall phase symmetry. However, SAXS and cryo-TEM measurements indicate that at least some Gd oleate exists as the bulk lamellar gel phase adopted by pure Gd oleate. This could exist as entirely separate domains of pure Gd oleate corresponding to the nonswelling lamellar nanoparticle structures observed by cryo-TEM in the dispersed samples. However, it may be possible for Gd oleate to exist as a separate mass within a Myverol-rich cubic domain. This could disrupt the structure to the extent that cubosome formation is prevented as observed. Such a structure could also explain the increased granularity of the bulk SAXS patterns, as the embedded Gd oleate may induce preferential alignment of the cubic domain around it. Finally cryo-TEM measurements suggest the presence of small numbers of residual cubosomes. This may indicate that, within this part of the structure, Gd oleate incorporation is at a low enough level that cubosome formation is not disrupted.

3.4. Gd Oleate Incorporation within Myverol: Effect on Relaxivity. Proton relaxivities, r_1 and r_2, of Myverol dispersions containing Gd oleate at various loadings were determined at 20 MHz (Figure 8). For T_1 measurements, the standard inversion−recovery (IR) method was used as the pulse sequence, and for T_2 measurements the Carr−Pucell−Meiboom−Gill (CPMG) method was used.[39] The longitudinal relaxivity, r_1, and transverse relaxivity, r_2, were then determined from the slope of the linear regression fits of $1/T_1$ and $1/T_2$ versus the Gd concentration, respectively.

Table 4 lists the particle size distribution and relaxivities of various Myverol/Gd oleate mixtures. Incorporation of Gd oleate within Myverol results in a marked increase in both r_1 and r_2 relative to pure Gd oleate. The relationship between the relaxivity and the weight ratio of Gd oleate is plotted in Figure 8. An initial sharp increase in relaxivity with weight percent Gd oleate is noted up to 1% Gd oleate. This increase is much more pronounced for the longitudinal relaxivity r_1. After this point, both the longitudinal and transverse relaxivity display a marked decrease with increasing Gd oleate content. By 50% Gd oleate in Myverol, the relaxivity is similar to that of pure Gd oleate.

We attempt to explain these trends with reference to the structural behavior described above. As described in the Introduction, contrast agents work by altering the relaxation times of water protons distributed around them. Around a paramagnetic ion, the relaxation rates of the bulk water are enhanced as a result of short-range interactions (inner-sphere relaxation from water molecules directly coordinated to the metal ions) and long-range interactions (outer-sphere relaxation from nearby H-bonded water). The latter are relatively small and are usually neglected. For paramagnetic materials, the inner-sphere relaxivity primarily results from a dipolar contribution (through-space interactions due to random fluctuations of the electric field) and can be described by the standard Solomon−Bloembergen−Morgan equation.[6]

$$\left(\frac{1}{T_1}\right)^{IS} = \frac{Cq}{55.5}\,\frac{1}{T_{1m}+\tau_m}$$

where $(1/T_1)^{IS}$, the observable NMR signal, is the relaxation rate of bulk solvent nuclei, C is the molal concentration of Gd, q is the number of bound waters per Gd (i.e., the number of inner-sphere

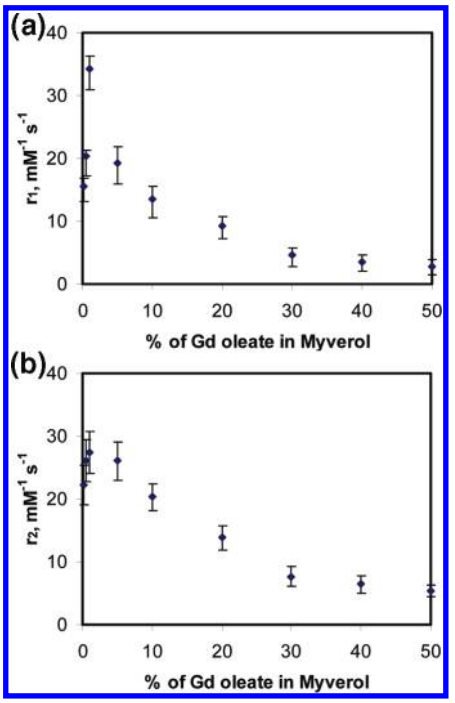

Figure 8. (a) Longitudinal r_1 and (b) transverse r_2 proton relaxivities as a function of weight percent Gd oleate in Myverol for dispersions of Myverol/Gd oleate. Relaxivities were determined at 20 mHz at room temperature.

waters), T_{1m} is the proton relaxation rate of bound water, and τ_m is the lifetime of water molecules in the inner sphere.

In general, when designing a new contrast agent, it is desirable to either increase the number of bound waters per Gd (q) or to increase the rotational correlation time of the paramagnetic ion (this decreases T_{1m}) while maintaining sufficient thermodynamic stability. DSC and SAXS results have shown that, in the bulk phase, Gd oleate is at least partially incorporated within the cubic phase of Myverol. The 3-D framework of the cubic phase with its continuous water networks and high surface area may facilitate the coordination of more water molecules around the Gd(III) ion. The ease with which water can move in the cubic phase may also lower τ_m, adding to the increase in relaxation rate. It may also impede the rotational movement of the metal ion, thereby improving the relaxation of water. Although SAXS and cryo-TEM data on the dispersed samples suggest that the cubic phase symmetry to a large extent is not retained upon dispersion, the fact that select dispersed samples, with low weight percent Gd oleate, exhibit increased relaxivity suggests that some localized structural elements of the cubic phase may have been retained within the colloidal particles (perhaps analogous to an L_3 phase).

The abrupt decrease in relaxivity as the Gd oleate loading increases from 1% to 5% has been previously observed for Gd incorporated within mesoporous silica[41] and for GdNaY nanoparticles[42] and explained with reference to the effect of increased Gd loading. It was suggested that at high Gd loading the dipole−dipole interaction among the metal ions becomes more significant, shortening the electronic relaxation and decreasing the overall relaxation rate.[41]

In this report, we have demonstrated the potential of Gd oleate loaded cubosomes to provide reasonable relaxivity values. We note, however, that Gd^{3+} toxicity is an important concern. As discussed in our previous paper on lanthanide oleates,[26] it is difficult to make a priori predictions of the chelation constants for the self-assembled lanthanide oleates as reaction equilibria constants in the interfacial microenvironment of amphiphile self-assembly materials can differ considerably from bulk solution values.[43] We will therefore address the issue of Gd ion toxicity in future work.

4. Conclusions

We have added Gd oleate to the cubic-forming Myverol system in excess water. DSC and SAXS measurements on the bulk systems indicate that Gd oleate is at least partially incorporated within the cubic phase of Myverol. However, at Gd oleate concentrations greater than 1 wt %, partial phase separation of the system may occur with the formation of a Gd-oleate-rich lamellar phase as well as the cubic phase. These bulk mixtures can be successfully dispersed into colloidal dispersions. Although the dispersion process appears to destroy the cubic phase in the presence of even the smallest amount of Gd oleate, we note that the relaxivities of select Gd oleate/Myverol systems are much higher than those of pure Gd oleate and the commercial contrast agent Magnevist, exemplifying the potential of this type of system for use in magnetic resonance imaging.

Acknowledgment. The authors thank Dr. David Cookson and Dr. Robert Knott for their assistance with experiments carried out at the ChemMatCARS beamline, sector 15 at the Advanced Photon Source. Use of the ChemMatCARS sector 15 at the Advanced Photon Source was supported by the Australian Synchrotron Research Program, which is funded by the Commonwealth of Australia under the Major National Research Facilities Program. ChemMatCARS Sector 15 is principally supported by the National Science Foundation/Department of Energy under Grant No. CHE-0535644. Use of the Advanced Photon Source was supported by the U.S. Department of Energy, Office of Science, Office of Basic Energy Sciences, under Contract No. DE-AC02-06CH11357. We acknowledge access to the SAXS camera owned by the School of Physics, Monash University. C.J.D. is the recipient of an Australian Research Council Federation Fellowship.

(41) Lin, Y. S.; Hung, Y.; Su, J. K.; Lee, R.; Chang, C.; Lin, M. L.; Mou, C. Y. *J. Phys. Chem. B* **2004**, *108*, 15608.

(42) Platas-Iglesias, C.; Vander Elst, L.; Zhou, W. Z.; Muller, R. N.; Geraldes, C. F. G. C.; Maschmeyer, T.; Peters, J. A. *Chem—Eur. J.* **2002**, *8*, 5121.

(43) Drummond, C. J.; Grieser, F.; Healy, T. W. *J. Chem. Soc., Faraday Trans. I* **1989**, *85*, 521.